Multiplexing of Fiber-Optic White Light Interferometric Sensors Using a Ring Resonator

Libo Yuan, Limin Zhou, Wei Jin, *Member, IEEE*, and M. S. Demokan, *Senior Member, IEEE*

***Abstract*—A single-mode fiber-optic ring resonator is used as a multipath reference for multiplexing white light interferometric sensors. The theory of applying the resonator for multiplexing Michelson-type interferometer sensor is presented. The capacity of the technique in terms of maximum sensor number is evaluated for both a linear array and a $M \times N$ sensor matrix. Experimental results for a three-sensor linear array and 2 × 1 sensor matrix are also presented.**

***Index Terms*—Multiplexing, optical fiber sensors, ring resonator, white light interferometry.**

I. Introduction

OPTICAL FIBER ring resonators have been used in a number of applications, including fiber ring lasers [1], [2], sensors [3], fiber laser gyroscopes [4], optical spectrum analyzers [5], [6], and optical delay lines [7]. In this paper, we report the use of a fiber ring resonator for a different application, i.e., to enhance the multiplexing capability of white light interferometric sensors.

White light interferometry, as a technique employing low-coherence broad-band light sources, has been a very active area of research within the past few decades [8]–[10]. The technique uses a scanning interferometer, e.g., a Michelson interferometer (MI), to match the optical path of signal light to that of reference light through the observation of white light interference fringes. The technique is capable of making absolute measurements with high resolution. The parameters that can be measured include position, displacement, strain, and temperature. White light interferometers can be configured to performed quasidistributed measurement by multiplexing a number of sensors on to a single fiber. However, switching between reference fibers of different lengths is required to match the optical paths of the reference signals to individual sensing signals [11]. The optical paths of the reference fibers are chosen to be approximately equal to that of the respective sensing signals to ensure they can be matched to each other by varying the optical path difference of the scanning interferometer over a reasonable distance. Scanning over an excessive distance is often difficult and accompanied with high cost and large power loss. A fiber ring resonator naturally generates light waves of multiple path lengths, and when it is placed in one arm of a scanning MI, the MI will act as an interferometer array. Each interferometer within the array is approximately matched to a particular sensor without needing to switch between different reference fibers.

Manuscript received December 17, 2001; revised April 30, 2002. This work was supported by the National Natural Science Foundation of China under Grant 50179007 by the Science Foundation of Heilongjiang Province for Outstanding Youth 1999, and the Foundation of Active Staff Support Program 2000, to the Harbin Engineering University and supported by the Hong Kong Polytechnic University under Grants G-W099 and G-Yc64.

L. Yuan is with the Department of Physics, Harbin Engineering University, Harbin 150001, China, and the Department of Mechanical Engineering, Hong Kong Polytechnic University, Hong Kong (e-mail: lbyuan@vip.sina.com).

L. Zhou is with the Department of Mechanical Engineering, Hong Kong Polytechnic University, Hong Kong.

W. Jin and M. S. Demokan are with the Department of Electrical Engineering, Hong Kong Polytechnic University, Hong Kong.

Digital Object Identifier 10.1109/JLT.2002.800800

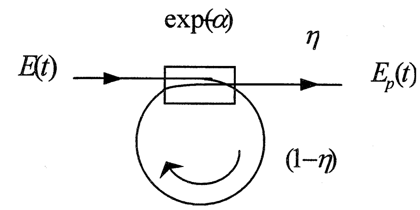

Fig. 1. Fiber-optic ring resonator.

This paper is organized as follows. The theory of the ring resonator as a multipath optical wave generator is presented in Section II. The multiplexing of a linear MI sensor array based on the ring resonator is discussed in Section III. Section IV discusses the extension of the multiplexing principle to sensor matrix .Section V discusses the multiplexing capacity in terms of maximum sensor number as a function of system parameters. Experimental results for a three-sensor linear array and a 2×1 sensor matrix are reported in Section VI. Finally, a brief summary concludes the paper.

II. Ring Resonator as a Multipath Lightwave Generator

Fiber-optic ring resonators, as shown in Fig. 1, are characterized by three basic parameters, the cavity length l_0, the splitting ratio of the loop coupler $\eta : (1-\eta)$, and the loss factor α of the fiber loop, including the insertion loss of the loop coupler.

Assume that the input field of the ring resonator is of the form

$$E_{\rm in}(k,t) = E_0(k)\exp(-jkct) \quad (1)$$

where E_0 is the amplitude, k is the wavenumber of the input wave, and c is speed of light in free space. The output field from the cavity may then be expressed as

$$E_{\rm out}(k,t) = E_0(k) \times \sum_{v=1}^{\infty}\left\{\exp(-v\alpha)\eta(1-\eta)^v \exp\left[-jk(ct - vnl_0)\right]\right\} \quad (2)$$

where n is the refractive index of the fiber core and v is the number of circulations through the fiber ring. The output is a summation of replica of the input wave with optical path delay $vnl_0 (v = 0, 1, 2, \ldots)$, representing a series of light waves.

III. Multiplexing of MI Sensor Array

Fig. 2 shows a multiplexed MI sensor array based on the ring resonator. A number of fiber segments are connected in serial to form a linear sensor array, which is further connected to a lead in/out fiber of length L_1. The ring resonator is inserted into the reference arm of the MI with a fiber length of L_0 (not including the resonator). The optical path length of the reference arm can be varied through the use of a gradient index (GRIN) lens–scanning mirror. The scanning mirror is used to adjust the optical path of the reference arm to match and trace the change of the fiber length in each sensing segment. When the optical path difference (OPD) between a sensing signal and a reference signal falls within the coherence length of the source, a white light fringe pattern is produced. The central fringe, which is located in the center of the fringe pattern and has the highest amplitude, corresponds to the exact path match of the two optical signals.

For a typical light-emitting diode (LED), its intensity distribution may be regarded to be of a Gaussian function [10]

$$\begin{aligned} I(k) =& E(k) \cdot E^*(k) \\ =& E_0(k) \cdot E_0^*(k) \frac{L_c}{\sqrt{2\pi}\xi} \exp\left[-\frac{L_c^2(k-k_0)^2}{2\xi^2}\right] \\ =& I_0 \frac{L_c}{\sqrt{2\pi}\xi} \exp\left[-\frac{L_c^2(k-k_0)^2}{2\xi^2}\right] \end{aligned} \quad (3)$$

where k is the wavenumber, L_c is the coherent length of the light signal, and ξ is a constant related to the spectral width of the light source.

For the multiplexed system as shown in Fig. 2, light from the source is split equally into two branches by a 3-dB coupler. The light signal from the sensing branch consists of $N+1$ reflected waves, corresponding to reflections at the $N+1$ joints of the N-segment sensing array, as shown in Fig. 3(a). The light field from the sensing branch as a function of wavenumber may be written as in (4), shown at the bottom of the page, where $\beta_i = 1 - \gamma_i, \gamma_i$ represents the excess loss associated with sensor i due to connection loss between the sensing segments. T_i and R_m are the transmission and reflection coefficient of the ith connector and mth partial reflector, respectively. T_i is generally smaller than $1 - R_i$ because of the loss factor γ_i. γ_i' and T_i' represent the loss and the transmission coefficient from the opposite direction, respectively.

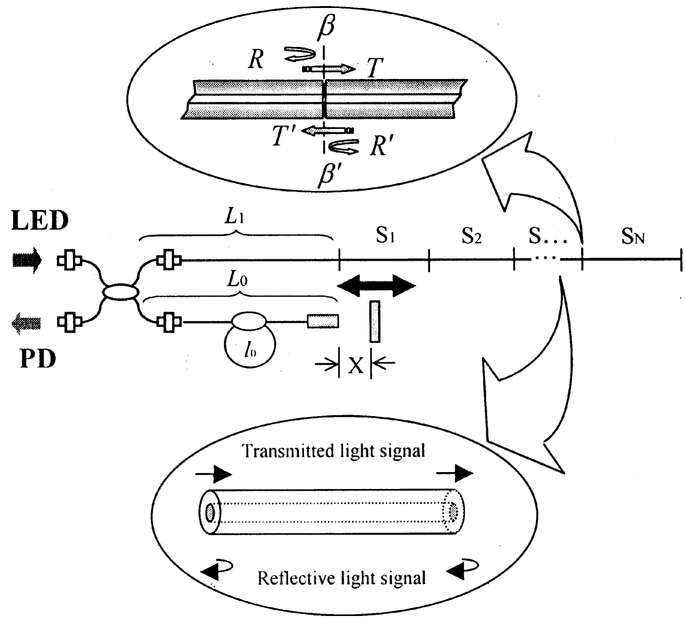

Fig. 2. Multiplexing MI array by a ring resonator.

Light signals from the reference branch are generated from the ring resonator and are illustrated in Fig. 3(b). The reference signal as a function of wavenumber can be expressed as in (5), shown at the bottom of the page, where R_0 is the reflectivity of the moving mirror and $f(X_v)$ is the loss associated with the scanning mirror–GRIN lens systems and is a function of X_v. The output light intensity with wavenumber k may be calculated as

$$\begin{aligned} I_A(k, X_v) =& [E_{As}(k,t) + E_{Ar}(k,t)] \cdot [E_{A_s}(k,t) + E_{Ar}(k,t)]^* \\ =& \frac{E(k)E^*(k)}{4} \\ & \times \sum_{m=0}^{N} \sum_{v=0}^{N} \left[B_m + C_v + 2\sqrt{B_m C_v} \cos(kx)\right] \end{aligned} \quad (6)$$

where

$$B_m = R_m \left[\prod_{i=0}^{m} T_i \beta_i T_i' \beta_i'\right]^2, \quad m = 0, 1, 2, \ldots, N \quad (7)$$

$$E_{As}(k,t) = \frac{E(k)}{2} \sum_{m=0}^{N} \left\{ \sqrt{R_m} \left[\prod_{i=1}^{m} T_i \beta_i T_i' \beta_i'\right] \exp\left[-jk\left(ct - 2nL_1 - 2n\sum_{i=1}^{m} l_i\right)\right]\right\} \quad (4)$$

$$E_{Ar}(k,t) = \frac{E(k)}{2} \sum_{v=0}^{\infty} \left\{ \sqrt{(v+1)R_0} f(X_v) \exp\left[-\left(\frac{v}{2}+1\right)\alpha\right] \eta(1-\eta)^{v/2} \exp\left[-jk\left(ct - 2nL_0 - vnl_0 - 2X_v\right)\right]\right\} \quad (5)$$

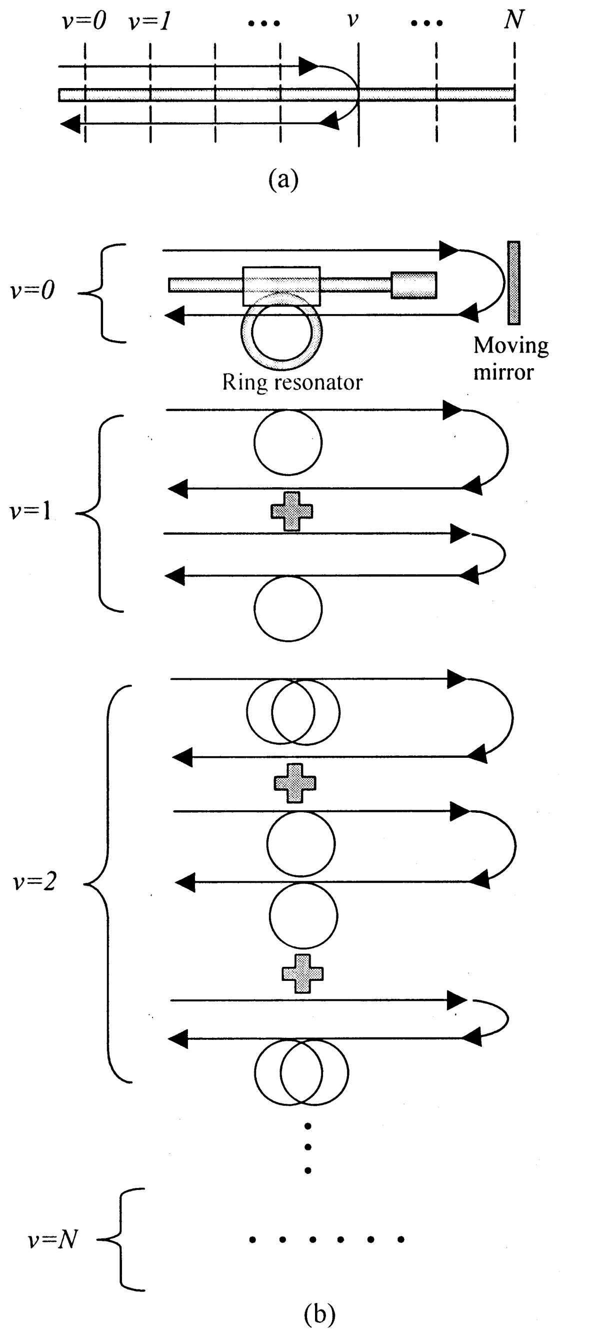

Fig. 3. (a) Reflected signals from the sensing arm. (b) Reflected signals from the reference arm containing the ring resonator.

$$C_v = (v+1)R_0 f^2(X_v)\exp[-(v+2)\alpha]\eta^2(1-\eta)^v, \quad v = 0,1,2,\ldots,N \tag{8}$$

and

$$x = 2X_v - 2n\left[(L_1-L_0)+\left(\sum_{i=1}^{m} l_i - v\frac{l_0}{2}\right)\right], \quad v = 0,1,2,\ldots,N. \tag{9}$$

The total output light intensity can be obtained by integrating (6) from $k=-\infty$ to $k=+\infty$ and can be expressed as in (10), shown at the bottom of the page. $I_A(X_v)$ would take nonzero value when and only when the following conditions are satisfied simultaneously:

$$m = v \tag{11}$$

$$|x| \le L_c. \tag{12}$$

$I_A(X_v)$ can then be rewritten as

$$I_A(X_v) = \frac{1}{4} \times \sum_{v=0}^{N}\int_{-\infty}^{+\infty} I(k)\left[B_v + C_v + 2\sqrt{B_v C_v}\cos(kx)\right]dk. \tag{13}$$

Substituting (3), (7), and (8) into (13) and letting $k' = k - k_0$, we may rewrite (13) as in (14), shown at the bottom of the next page. There are $N+1$ terms in the right-hand side (RHS) of (14), corresponding to $N+1$ sets of interferometric signals. From (14), it can be seen that $N+1$ white light interference patterns can be generated if X_v is varied through the use of the scanning mirror, corresponding to x in (14) [defined by (9)], which equals zero for $v = 0,1,2,\ldots,N$.

This multiplexed sensor array can be used to perform quasidistributed strain or temperature measurements [12]. Since the centers of the $N+1$ white light fringe patterns, where the amplitudes are maximized, are corresponding to $x=0$, the value of X_v at the central maximum may be obtained by setting $x=0$ in (9) and can be expressed as

$$X_v = n\left[(L_1-L_0)+\sum_{i=1}^{v}\left(l_i - \frac{l_0}{2}\right)\right], \; v = 0,1,2,\ldots,N. \tag{15}$$

If $|n(l_i - l_j)|, (i \ne j)$, and $|n(l_i - l_0/2)|$ are further chosen to be larger than the coherence length of the light source, the value of X_v for a different v would change, corresponding to the interferograms produced by the various sensing and referencing wave pairs not overlapping. The difference $\Lambda_v = X_v - X_{v-1}$ can be calculated from (15) and expressed as

$$\Lambda_v = n\left(l_v - \frac{l_0}{2}\right). \tag{16}$$

$$I_A(X_v) = \int_{-\infty}^{+\infty} I_A(k, X_v)dk = \frac{1}{4}\sum_{m=0}^{N}\sum_{v=0}^{N}\int_{-\infty}^{+\infty} I(k)\left[B_m + C_v + 2\sqrt{B_m C_v}\cos(kx)\right]dk \tag{10}$$

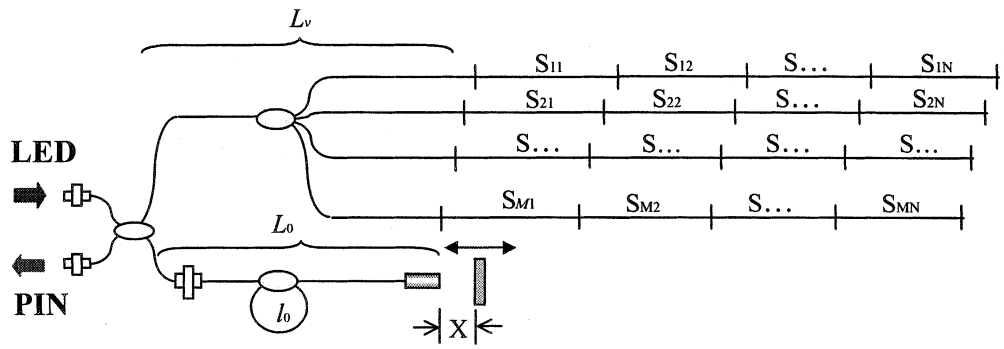

Fig. 4. Configuration of multiplexed MI matrix.

Assume that l_v is changed to $l_v + \Delta l_v$ due to a strain applied to sensor v, the measured change in Λ_v (i.e., $\Delta\Lambda_v$) may be related to the applied strain by

$$\Delta\Lambda_v = n\Delta l_v = n l_v \varepsilon_v \tag{17}$$

where $\varepsilon_v = \Delta l_v / l_v$ is the strain applied to sensor v. If the variations in X_v $(v = 0, 1, \ldots, N)$ are measured and recorded, the strains applied to all the sensors can be recovered by using (17).

IV. Multiplexing of MI Sensor Matrix

The ring-resonator technique can be further extended to the multiplex fiber-optic MI matrix through the use of a $1 \times M$ star coupler. The schematic of such a system is shown in Fig. 4. The system is basically the same as in Fig. 2 but with the linear sensor array replaced by an $M \times N$ sensor matrix. Each branch of the $1 \times M$ star coupler is a $1 \times N$ sensor array, formed by connecting N sensing fiber segments in serial. The gauge length of sensor S_{uv} is $l_{uv}(u = 1, 2, 3, \ldots, M; v = 0, 1, 2, \ldots, N)$. The sensor interrogation is still accomplished by the use of the scanning mirror.

As shown in Fig. 4, the optical path of the reflected signal from the joint between sensors S_{uv-1} and S_{uv} is

$$2nL_u + 2n\sum_{i=1}^{v} l_{ui}, \begin{cases} u = 1, 2, 3, \ldots, M \\ v = 0, 1, 2, \ldots, N \end{cases}. \tag{18}$$

The light field reflected from the sensor array at the photodiode can be expressed as in (19), shown at the bottom of the page, where R_{uv} represents the reflectivity at the joint between S_{uv-1} and S_{uv}. The optical paths of the reference signals generated from the ring resonator are

$$2nL_0 + vnl_0 + 2X_{uv}, \begin{cases} u = 1, 2, 3, \ldots, M \\ v = 0, 1, 2, \ldots, N \end{cases}. \tag{20}$$

The reference light field at the photodetector is shown in (21), appearing at the bottom of the page.

$$\begin{aligned} I_A(X_v) =& \frac{1}{4}\sum_{v=0}^{N}\int_{-\infty}^{+\infty}\left\{I_0\frac{L_c}{\sqrt{2\pi}\xi}\exp\left[-\frac{L_c^2 k'^2}{2\xi^2}\right]\right\}\left\{B_v + C_v + 2\sqrt{B_v C_v}\cos[(k'+k_0)x]\right\}dk' \\ =& \frac{I_0}{4}\sum_{v=0}^{N}\int_{-\infty}^{+\infty}\left\{\frac{L_c}{\sqrt{2\pi}\xi}\exp\left[-\frac{L_c^2 k'^2}{2\xi^2}\right]\right\}\left\{B_v + C_v + 2\sqrt{B_v C_v}\left[\cos(k'x)\cos(k_0 x) - \sin(k'x)\sin(k_0 x)\right]\right\}dk' \\ =& \frac{I_0}{4}\sum_{v=0}^{N}\left\{B_v + C_v + 2\sqrt{B_v C_v}\exp\left(-\frac{\xi^2}{2L_c^2}x^2\right)\cos(k_0 x)\right\} \end{aligned} \tag{14}$$

$$E_{Ms}(k,t) = \frac{E(k)}{2}\sum_{u=1}^{M}\sum_{v=0}^{N}\left\{\frac{\sqrt{R_{uv}}}{M}\left[\prod_{i=1}^{v} T_{ui}\beta_{ui}T'_{ui}\beta'_{ui}\right]\exp\left[-jk\left(ct - 2nL_u - 2n\sum_{i=1}^{v} l_{ui}\right)\right]\right\} \tag{19}$$

$$E_{Mr}(k,t) = \frac{E(k)}{2}\sum_{u=1}^{M}\sum_{v=0}^{N}\left\{\sqrt{(v+1)R_0}f(X_{uv})\exp\left[-\left(\frac{v}{2}+1\right)\alpha\right]\eta(1-\eta)^{v/2}\exp\left[-jk\left(ct - 2nL_0 - vnl_0 - 2X_{uv}\right)\right]\right\} \tag{21}$$

By following a similar process to the derivation of (14), we obtain the output light intensity of the $M \times N$ sensor matrix as shown in (22) at the bottom of the page, where

$$B_{uv} = \frac{R_{uv}}{M^2}\left[\prod_{i=1}^{v} T_{ui}\beta_{ui}T'_{ui}\beta'_{ui}\right]^2, \quad \begin{cases} u = 1,2,3,\ldots,M \\ v = 0,1,2,\ldots,N \end{cases} \tag{23}$$

$$C_{uv} = (v+1)R_0 f^2(X_{uv})\exp[-(v+2)\alpha]\eta^2(1-\eta)^v, \quad \begin{cases} u = 1,2,3,\ldots,M \\ v = 0,1,2,\ldots,N \end{cases} \tag{24}$$

$$x' = 2X_{uv} + 2n(L_0 - L_u) + 2n\sum_{i=1}^{v}\left(\frac{l_0}{2} - l_{ui}\right), \quad \begin{cases} u = 1,2,3,\ldots,M \\ v = 0,1,2,\ldots,N \end{cases}. \tag{25}$$

From (22), it can be seen that $M \times (N+1)$ interference peaks can be obtained by varying the OPD of the MI through the use of the scanning mirror. The difference in the peak positions $\Lambda_{uv} = X_{uv} - X_{u,v-1}$ can be obtained from (25) by setting $x' = 0$ as

$$\Lambda_{uv} = n\left(l_{uv} - \frac{l_0}{2}\right). \tag{26}$$

The matrix system can be used to measure the strain or temperature distribution over a grid of points. We take temperature measurement as an example. Assume that at temperature T_0, the optical path length of sensor S_{uv} is $n(T_0)l_{uv}(T_0)$. Due to thermal expansion and the change of the fiber index with temperature, the optical path length will be different at T_{uv}. The variation of Λ_{uv} due to variation of temperature from T_0 to T_{uv} can be derived from (26) as

$$\Delta\Lambda_{uv} = n(T_0)l_{uv}(T_0)\left[\alpha_T + C_T\right](T_{uv} - T_0) \tag{27}$$

where $n(T_0)$ is the refractive index of fiber at temperature T_0. α_T and C_T are the thermal expansion coefficient and the thermal-optic coefficient of the optical fiber, respectively. Since $\Delta\Lambda_{uv}$ can be obtained from the measurement of the positions of the scanning mirror that corresponds to the maxima of the interferometric fringes, the temperature distribution T_{uv} can then be calculated as

$$T_{uv} = \frac{\Delta\Lambda_{uv}}{n(T_0)l_{uv}(T_0)[\alpha_T + C_T]} + T_0, \quad \begin{cases} u = 1,2,3,\ldots,M \\ v = 0,1,2,\ldots,N \end{cases}. \tag{28}$$

For standard commercial communication single-mode fiber at wavelength $\lambda = 1300$ and 1550 nm, the parameters are $n = 1.4681$ (at $T = 25°$C), $\alpha_T = 5.5 \times 10^{-7}/°$C, $C_T = 0.762 \times 10^{-5}/°$C, and $n = 1.4675$ (at $T = 25°$C), $\alpha_T = 5.5 \times 10^{-7}/°$C, $C_T = 0.811 \times 10^{-5}/°$C [13], respectively.

V. Evaluation of Multiplexing Capability

Assume that the light power launched into the fiber is I_0, and the minimum power variation that can be detected by the photodiode is $I_{\min}$. The maximum sensor number that can be multiplexed can be evaluated by using

$$I_D(u,v) \geq I_{\min}, \quad \begin{cases} u = 1,2,3,\ldots,M \\ v = 0,1,2,\ldots,N \end{cases} \tag{29}$$

where $I_D(u,v)$ is the power variation at the photodetector due to sensor S_{uv}. For the linear sensor array, the magnitude of power variation of sensor $v (v = 0,1,2,\ldots,N)$ can be obtained from (14) as

$$\begin{aligned} I_{AD}(X_v)|_{x=0} &= \frac{I_0}{2}\sqrt{B_v C_v} \\ &= \frac{I_0}{2}\left\{R_v\left[\prod_{i=0}^{v} T_i\beta_i T'_i\beta'_i\right]^2 (v+1)\right. \\ &\quad \times R_0 f^2(X_v)\exp[-(v+2)\alpha] \\ &\quad \left.\times \eta^2(1-\eta)^v\right\}^{1/2}. \end{aligned} \tag{30}$$

The peak power variation for the sensor matrix can be obtained from (22) as

$$\begin{aligned} I_{MD}(X_{uv})|_{x'=0} &= \frac{I_0}{2}\sqrt{B_{uv} C_{uv}} \\ &= \frac{I_0}{2}\left\{\frac{R_{uv}}{M^2}\left[\prod_{i=1}^{v} T_{ui}\beta_{ui} T'_{ui}\beta'_{ui}\right]^2 (v+1)\right. \\ &\quad \times R_0 f^2(X_{uv})\exp[-(v+2)\alpha] \\ &\quad \left.\times \eta^2(1-\eta)^v\right\}^{1/2}. \end{aligned} \tag{31}$$

To estimate the number of sensors that can be multiplexed using the ring-resonator technique, we conducted a computer simulation using (30) and (31). During simulation, we assumed that the average attenuation between the moving mirror and the GRIN lens collimator is 6 dB, i.e., $f(X_p) = f(X_{uv}) = 1/4$. The excess loss of the 3-dB coupler was neglected while the excess loss of the loop coupler forming the ring resonator was taken as $\alpha = 0.06$ dB. Other parameters used in the simulation are $\beta_v = \beta_{uv} = \beta'_v = \beta'_{uv} = 0.9$; $T_v = T_{uv} = T'_v = T'_{uv} = 0.89$; and $R_v = R_{uv} = 1\%$ ($u = 1,2,\ldots,M; v = 0,1,2,\ldots,N$) and $R_0 = 91\%$.

Fig. 5 shows the output signal intensity (normalized) for each of the sensors within an array of ten sensors for $\eta = 0.3$. The typical detecting capability of the photodiode is about 1 nW. Taking into account the possible system noise, a reasonable detect limit may be assumed to be $I_{\min} = 5$ nW. For a source power level of $I_0 = 50\ \mu$W, the maximum sensor number satisfying (29) is $N_{\max} = 3$, corresponding to three fiber-optic sensors connected in serial. For $I_0 = 3$ mW, the sensor number can be increased to $N_{\max} = 15$.

$$I_M(X_{uv}) = \frac{I_0}{4}\sum_{u=1}^{M}\sum_{v=0}^{N}\left\{B_{uv} + C_{uv} + 2\sqrt{B_{uv}C_{uv}}\exp\left(-\frac{\xi^2}{2L_c^2}x'^2\right)\cos(k_0 x')\right\} \tag{22}$$

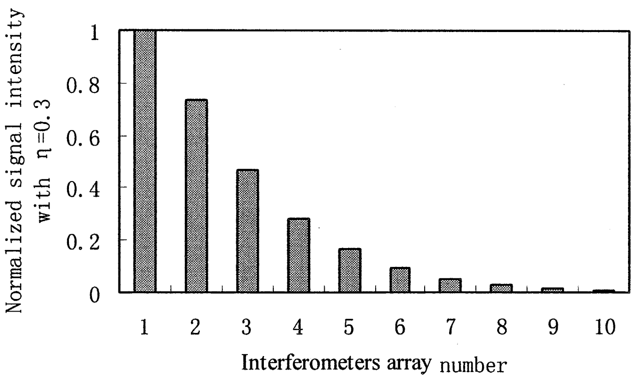

Fig. 5. Intensity distribution (normalized by I_0) of the sensors within a ten-sensor line array ($\eta = 0.3$).

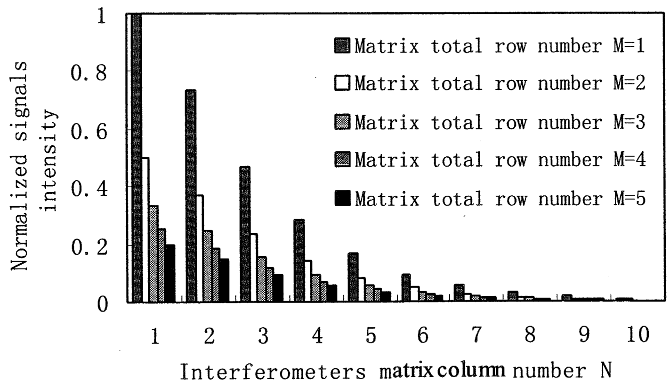

Fig. 7. Intensity distribution of the sensors within the first branch of the $1 \times M$ coupler when the matrix size is varied from 1×10 to 5×10.

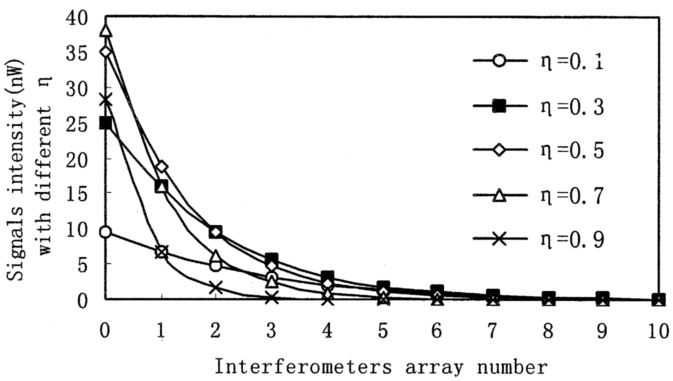

Fig. 6. Intensity distribution of sensors within a line array for a varying coupling rate from $\eta = 0.1$ to $\eta = 0.9$ ($I_0 = 50\,\mu W$).

It should be mentioned that the maximum sensor number, as discussed previously, is affected by the coupling ratio $\eta : (1-\eta)$ of the loop coupler. Fig. 6 shows the signal intensity of individual sensors in the ten-sensor array when η is varied from 0.1 to 0.9 for an input power level of $I_0 = 50$ μW. The optimal result is approximately $\eta = 0.3$. For $\eta = 0.9$, the sensor number with the previously set detection limit ($I_{\min} = 5$ nW) is reduced to two.

The normalized output intensities of sensors within the first branches of an $M \times 10$ matrix for $M = 1, 2, \ldots, 5$ were calculated by using (31) for $\eta = 0.3$. The results are shown in Fig. 7. During calculation, the star coupler was assumed to split power equally into the M branches, and the insertion loss of the star coupler is negligible. As expected, the intensity level decreases when the numbers of branches are increased. For the input power level of $I_0 = 50$ μW and $I_0 = 3$ mW, the maximum sensor number was calculated to be $M \times N|_{\max} = 2 \times 2$ (four sensors) and $M \times N|_{\max} = 3 \times 3$ (nine sensors) or 4×2 (eight sensors), respectively.

It should be mentioned that the maximum sensor number is also limited by the scanning distance of the scanning mirror. Consider a linear array with sensor gauge length satisfying $l_1 < l_2 < \cdots < l_N$ over the entire measurement range. The maximum sensor number will be determined by $X_{v,\max}/\max_{i=1,2,\ldots,N-1}\{l_{i+1} - l_i\}$, where $X_{v,\max}$ is the maximum scanning distance and $\max_{i=1,2,\ldots,N-1}\{l_{i+1} - l_i\}$ is the maximum difference in the gauge lengths of adjacent sensors. For $X_{v,\max} = 20$ cm and $\max_{i=1,2,\ldots,N-1}\{l_{i+1} - l_i\} = 5$ mm, the maximum sensor number is 40.

VI. Experiments and Results

Experiments were conducted with a three-sensor linear array and a 2×1 sensor matrix. The light source used in the experiments was an LED source with a power of 50 μW and a center wavelength of 1310 nm. The insertion loss of the scanning mirror–GRIN lens combination varied from a 4-dB to an 8-dB change as the gap distance between the fiber-optic collimator and the scanning mirror was varied from 3 to 150 mm. The reflectivity of the scanning mirror is 91%. The insertion loss α and the coupling ratio $\eta : (1-\eta)$ of the loop coupler forming the resonator are approximately 0.06 dB and 3:7, respectively. The gauge lengths of the sensors were chosen to be slightly different from each other but approximately equal to 100 mm. The cavity length l_0 of the ring resonator was chosen to be approximately twice that of the sensor gauge lengths. The different gauge lengths ensure that the interferogram for each sensor is unique and not overlapping with other sensors. For the linear array, the reference arm L_0 was chosen to be slightly shorter than the sensing arm L_1 (approximately 2 mm), allowing for the path match of the two arms by varying X_v. For the 2×1 matrix system, a 1×2 star coupler is used to split the sensing signal into two arms. The lengths of the two arms ($L_u, u = 1, 2$) are chosen to be slightly longer than the reference arm L_0. The photodetector output for the 1×3 and 2×1 sensor array are shown in Figs. 8 and 9, respectively.

In Fig. 8, the fringe identified as $v = 0$ is due to the reflection occuring at the joint between the first sensor and the lead in/out fiber. The fringes identified as $v = 1$, 2, and 3 are due to the reflections at the joints between the second and the first, the third and the second, and the far end of the third sensors, respectively. The distances between the peak positions S_1, S_2, and S_3, as shown in Fig. 8, are proportional to the gauge lengths of sensor 1, 2, and 3, respectively. Fig. 9(a) shows one of the two branches of the 2×1 sensor matrix; the peaks of approximately 550 and 1550 mm are due to the reflection at the joint between the sensor and the lead in/out fiber and the reflection at the far end of the sensing fiber, respectively. For the 2×1 sensor matrix, the differences S_{21} and S_{22}, shown in Fig. 9(b), are measures of the sensor gauge lengths.

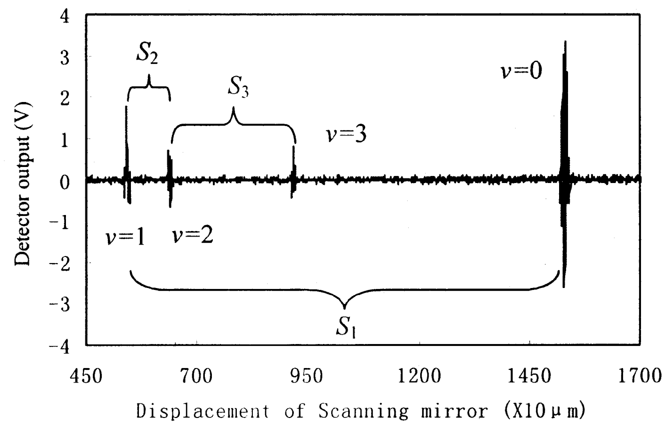

Fig. 8. Photodetector output of the three-sensor linear array when the mirror was scanned from 4.5 to 17 mm at a speed of 2 mm/s.

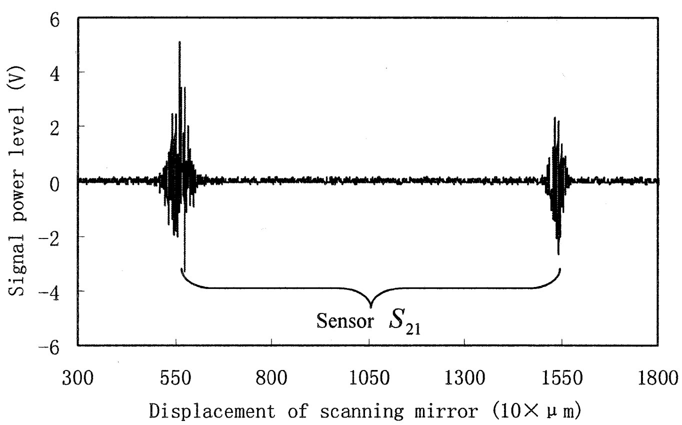

(a)

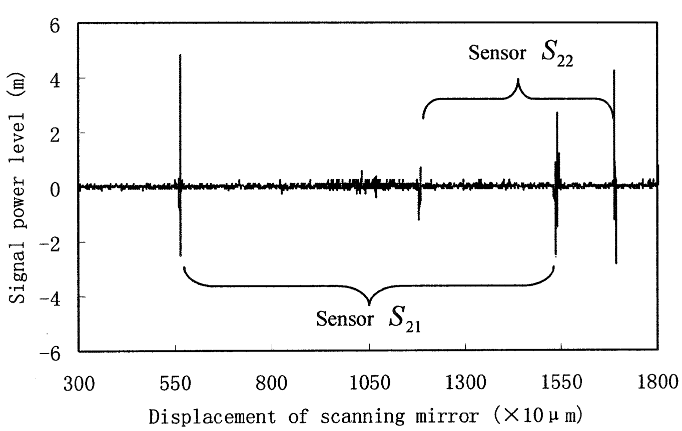

(b)

Fig. 9. Photodetector output of a 2 × 1 interferometer matrix when the mirror was scanned from 3 to 18 mm. (a) Only one sensor in the first branch is connected (mirror scanning speed is 1 mm/s). (b) Sensors in both branches are connected (mirror scanning speed is 10 mm/s).

VII. Conclusion

We have investigated the use of a ring resonator for multiplexing fiber-optic Michelson-type white light interferometers. Formula related the peak intensity of the interference fringes, and the system parameters were derived. Based on this multiplexing technique, the capability of maximum sensor number was evaluated. It was found that, in the condition of 3-mW light source power, it is possible to multiplex 15 sensors in a linear array or 9 sensors in an $M \times N$ matrix configuration. Experimental results with a three-sensor linear and 2×1 sensor matrix support the theoretical predictions. The technique can be used for quasidistributed strain or temperature measurement for smart structures applications.

References

[1] K. O. Hill, B. S. Kawasaki, and D. C. Johnson, "CW Brillouin laser," *Appl. Phys. Lett.*, vol. 28, pp. 608–609, 1976.

[2] L. F. Stokes, M. Chodorow, and H. J. Shaw, "All-fiber stimulated Brillouin ring laser resonator with submilliwatt pump threshold," *Opt. Lett.*, vol. 7, pp. 509–511, 1982.

[3] D. A. Jackson and J. D. C. Jones, "Fiber-optic sensors," *Optica Acta*, vol. 33, pp. 1469–1503, 1986.

[4] F. Zarinetchi, S. P. Smith, and S. Ezekiel, "Stimulated Brillouin fiber-optic laser gyroscope," *Opt. Lett.*, vol. 16, pp. 229–231, 1991.

[5] K. Kalli and D. A. Jackson, "Ring resonator optical spectrum analyzer with 20 kHz resolution," *Opt. Lett.*, vol. 17, pp. 1090–1092, 1992.

[6] S. Tai, K. Kyuma, and T. Nakayama, "Novel measuring method for spectral linewidth of laser diodes using fiber-optic ring resonators," *Electron. Lett.*, vol. 21, pp. 91–93, 1985.

[7] S. A. Newton, R. S. Howland, K. P. Jackson, and H. J. Shaw, "High-speed pulse-train generation using single-mode fiber recirculating delay lines," *Electron. Lett.*, vol. 19, pp. 757–758, 1983.

[8] S. A. Al-Chalabi, B. Culshaw, and D. E. N. Davies, "Partially coherent sources in interferometry," in *Proc. 1st Int. Conf. Optical Fiber Sensors*, London, U.K., 1983, pp. 132–135.

[9] T. Bosselman and R. Ulrich, "High accuracy position-sensing with fiber-doupled white light interferometers," in *Proc. 2nd Int. Conf. Optical Fiber Sensors*, Stuttgart, Germany, 1984, pp. 361–365.

[10] L. B. Yuan, "White light interferometric fiber-optic strain sensor with three-peak-wavelength broadband LED source," *Appl. Opt.*, vol. 36, no. 25, pp. 6246–6250, 1997.

[11] L. B. Yuan and F. Ansari, "White-light interferometric fiber-optic distributed strain-sensing system," *Sens. Actuators*, vol. A63, pp. 177–181, 1997.

[12] L. B. Yuan, L. M. Zhou, and W. Jin, "Quasidistributed strain sensing with white-light interferometry: A novel approach," *Opt. Lett.*, vol. 25, no. 15, pp. 1074–1076, 2000.

[13] L. B. Yuan, "Effect of temperature and strain on fiber-optic refractive index," *Acta Optica Sinica*, vol. 17, pp. 1713–1717, 1997.

Libo Yuan, photograph and biography not available at time of publication.

Limin Zhou, photograph and biography not available at time of publication.

Wei Jin (S'99–M'00), photograph and biography not available at time of publication.

M. S. Demokan (SM'89), photograph and biography not available at time of publication.